Estimation of the Average Power Density in the Vicinity of Cellular Base-Station Collinear Array Antennas

Antonio Faraone, *Member, IEEE*, Roger Yew-Siow Tay, *Member, IEEE*, Ken H. Joyner, and Quirino Balzano, *Senior Member, IEEE*

***Abstract*—This paper investigates the character of the average power density in the close proximity of base-station antennas, where human exposure to electromagnetic fields radiated from such radio-frequency (RF) sources is the highest. The concept of average power density is used since, in proximity of a large array antenna, the direction of the power flow at a given point is not readily predictable because of the substantially diverging path lengths and direction of propagation of the energy arriving from different array elements. This quantity is shown to have a marked cylindrical decay near the antennas, which converts to spherical in the far field. On this basis, a set of simple prediction formulas is derived to allow the estimation of the average power density with good precision. The latest IEEE C95.1-1999 Standard for RF safety calls for spatially averaged measurements of incident power density to verify compliance to maximum permissible exposure limits. The advantage of using the concept of average power density and the resulting prediction formulas is that the evaluation of the exposure of humans near cellular base-station antennas becomes extremely simple during surveys when large computerized scanning equipment may not be available.**

***Index Terms*—Base-station antenna, collinear array, human exposure, RF dosimetry.**

I. Introduction

WITH the proliferation of cellular base-station sites, there has been concern for the potential exposure of personnel who might come in close proximity of radiating antennas. There are safety standards for the exposure of humans in the "controlled" or working place environment [1]. The exposure is quantified both in terms of radio-frequency (RF) power absorbed by the exposed human and of incident power density. The power absorbed by the humans in a RF field can be measured by using laboratory methods [2], [3], or it can be estimated by using numerical methods, which have been tabulated if the exposure is in the far field of RF sources [4]. The exposures of most concern are seldom in the far field of antennas, because the distance from the radiators reduces the incident RF energy flow to a level below safety limits, unless we are dealing with extraordinarily powerful transmitters, e.g., radar.

Cellular base-station communication systems often have high-gain antennas, e.g., collinear arrays 2–3 m long, and relatively low total power transmitted (<1 kW). In these conditions, if there is access to the antenna installation, as for maintenance personnel, the highest RF exposure is in the immediate vicinity of the array, which might be approachable.

Regarding the effects in the following discussion, we can assume that the exposure of interest is in the near field of array antennas, but at distances that are of the order of magnitude of a radiating element size ($\approx\lambda/2$) or greater. If this is the case, the radiation impedances of the antenna elements are not radically affected by the presence of a person, and the power radiated by the antenna is not significantly different from free-space condition. In other words, the energy scattered and reflected by the human changes the radiation pattern of the antenna, but not its matching. For closer distances, tighter coupling with individual radiators can cause a mismatch of the driving point impedance of the antenna elements, change the antenna excitation profile, and alter substantially the power radiated by the antenna. In our analysis, we make the hypothesis that the presence of the human does not change substantially the RF current on the individual radiating elements of the array antenna.

Human exposure is quantified by the distribution of the time derivative of absorbed electromagnetic energy per unit mass, i.e., *specific absorption rate* (SAR) [1], within the exposed body caused by the incident fields. SAR measurements require sophisticated experimental or analytical methods to acquire results [2], [3], [5], [6]. In survey situations, where E- or H-field sensors are available, the only parameters that can be evaluated are the local electric ($|\boldsymbol{E}|^2$) and/or magnetic ($|\boldsymbol{H}|^2$) field amplitude square. At a large distance from RF antennas, the electric and magnetic field amplitudes are related to each other in a simple fashion through the free-space impedance and to the incident RF power density, which in turn can be used to quantify the peak and average SAR of the exposure [7]. In the case of cellular base-station installations (as with many RF sources), the highest intensity of $|\boldsymbol{E}|^2$ and $|\boldsymbol{H}|^2$ is found close to the antennas in regions where free-space propagation cannot be assumed. In these conditions, we cannot accept that the measurement of $|\boldsymbol{E}|^2$ and/or $|\boldsymbol{H}|^2$ are simply related to incident power density. Safety standards allow explicitly $|\boldsymbol{E}|^2$ measurements for compliance purpose [7], [8].

There are several available E-field survey meters [9] that are routinely employed to assess the safety of RF exposure in proximity of cellular base-station antennas, although the readings are not always simply related to the incident RF power density. We will examine the significance of $|\boldsymbol{E}|^2$ measurements near a

Manuscript received July 9, 1998; revised June 30, 1999.

The authors are with Motorola Florida Research Labs, Fort Lauderdale, FL 33322 USA (e-mail: eaf006@email.mot.com).

Publisher Item Identifier S 0018-9545(00)03685-9.

0018–9545/00$10.00 © 2000 IEEE

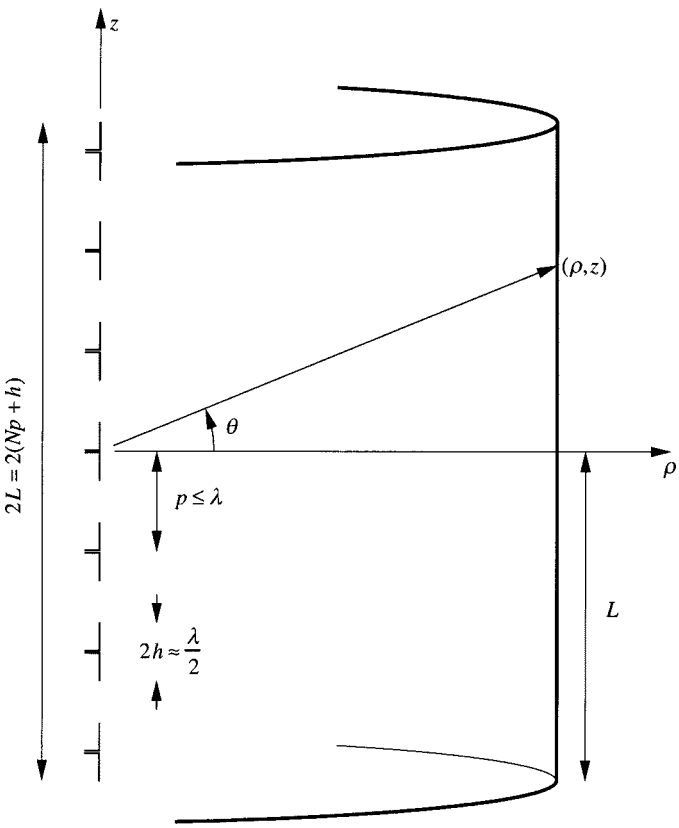

Fig. 1. A collinear array of half-wave dipoles enclosed in the intercepting cylindrical surface where the power density is averaged. The relevant reference frames are established.

base-station antenna (collinear array or other) in terms of their relation to the average power density. The purpose of this paper is to show that the average power density along the array height is the most convenient observable quantity to assess the exposure from cellular basestation antennas. This assessment method is in agreement with the latest version of the IEEE C95.1-1999 for the safe exposure of humans to RF electromagnetic energy. The recent ICNIRP guidelines [8] also call for averaging of the electromagnetic fields over the body of the exposed person, although the averaging method is not specified.

The format of this paper is as follows. In Section II, theoretical considerations lead us to define the character of the electromagnetic field radiated by a collinear array. In Section III, we discuss the significance of electric energy density measurements near cellular basestation antennas and how they relate to safety surveys. In Section IV, we establish some simple formulas that allow the prediction of the actual exposure with remarkable accuracy. These formulas are validated on measurements of practical array configurations.

II. Theoretical Considerations: Collinear Arrays

A. Average Power Density

Consider the collinear array of half-wave dipoles in Fig. 1. The array consists of $2N+1$ radiating elements, each excited by a time-harmonic current of amplitude I_n; the elements are spaced by the distance p ($\leq\lambda$ at the highest operating frequency of the antenna) along the z axis. The antenna has a length $2L$, and each half-wave radiator is $2h$ long ($2h=\lambda/2$ at the center frequency of operation). Given the rotational symmetry of the structure, the power flow through a lateral cylindrical surface at a distance ρ from the axis of the array is found using the Poynting theorem for time-harmonic electromagnetic fields

$$\begin{aligned} 2\pi\rho \int_{-\infty}^{+\infty} \mathrm{Re}\{\tfrac{1}{2}\,\boldsymbol{E}\times\boldsymbol{H}^*\cdot\hat{\boldsymbol{\rho}}\}\,dz &= 2\pi\rho \int_{-\infty}^{+\infty} \mathrm{Re}\{\tfrac{1}{2}\,E_z H_\phi^*\}\,dz \\ &= P_{\mathrm{rad}} \end{aligned} \tag{1}$$

where

P_{rad}	power radiated by the array;
$\hat{\boldsymbol{\rho}}$	unit vector in the radial direction;
E_z	z component of the electric field;
H_ϕ^* ($\hat{\boldsymbol{\phi}}=\hat{\boldsymbol{z}}\times\hat{\boldsymbol{\rho}}$)	complex conjugate amplitude of the only component of the magnetic field.

Since practically no power is radiated in the directions close to the axis of the antenna, for distances $\rho \ll L$ (but still $>\lambda/2$), (1) can be rewritten

$$2\pi\rho \int_{-L}^{L} \mathrm{Re}\{\tfrac{1}{2}\,E_z H_\phi^*\}\,dz \approx P_{\mathrm{rad}}. \tag{2}$$

If we average the result over a straight line belonging to the cylindrical surface enclosing the array and we call $\overline{P}_d$ the average power density there, then

$$\overline{P}_d(\rho) \approx \frac{P_{\mathrm{rad}}}{2L\cdot 2\pi\rho}. \tag{3}$$

Geometrically, (3) states that as long as the power radiated through the top and the bottom of the cylindrical surface enclosing the array can be neglected, the average power density decays with the inverse of the distance from the antenna. Equation (3) is significant because it can be used to check the validity of survey results with a simple arithmetical operation, if P_{rad}, ρ, and L are known. A similar trend was extrapolated in [10] from on-site surveys; however, the *average* power density was not taken as the observable quantity, as the extrapolation was based on measured data taken at single field points. Equation (3), however, fails to give any information about the vertical distribution of $P_d=(1/2)\,\mathrm{Re}\{E_z H_\phi^*\}$ at any distance ρ, or when the propagating wave eventually becomes spherical.

The cylindrical character of the electromagnetic field in the immediate vicinity of the array can be seen using the simple and elegant solution for the field radiated from a half-wave dipole established by Jordan and Balmain [11]. The total H-field is given by the superposition of the contribution of each radiator

$$\begin{aligned} H_\phi(\rho,z) &= \sum_{n=-N}^{N} H_{\phi,n}(\rho,z) \\ &= \sum_{n=-N}^{N} j\,\frac{I}{4\pi\rho}\,[e^{-j\beta R_{1,n}} + e^{-j\beta R_{2,n}}] \end{aligned} \tag{4}$$

with $\beta=2\pi/\lambda$ and

$$R_{1,n} = \sqrt{\rho^2+(z-np-h)^2} \tag{5a}$$

$$R_{2,n} = \sqrt{\rho^2+(z-np+h)^2} \tag{5b}$$

where, in a first approximation, we have set $I_n = I$. In this frame, we purposely neglect the mutual interaction between array elements in order to approach the problem in simple analytical terms. As it will be clear later, neglecting mutual coupling does not compromise the generality of the results that will be derived. The main effect of mutual coupling on collinear half-wave dipoles fed in phase is to lower the radiation resistance a few ohms [12]. As long as the feed-point currents have similar magnitude, this effect can be estimated to raise the feed-point current roughly 5–10%, depending on the number of adjacent elements. The E-field can be expressed as

$$\begin{aligned}\boldsymbol{E}(\rho, z) &= \hat{\boldsymbol{\rho}} E_\rho(\rho, z) + \hat{\boldsymbol{z}} E_z(\rho, z) \\ &= \frac{1}{j\omega\varepsilon_0}\left\{-\hat{\boldsymbol{\rho}}\frac{\partial}{\partial z} H_\phi(\rho, z) + \hat{\boldsymbol{z}}\frac{1}{\rho}\frac{\partial}{\partial \rho}[\rho H_\phi(\rho, z)]\right\}\end{aligned} \tag{6}$$

where ω is the angular frequency of operation and ε_0 the permittivity of free space. Since we are interested in the distribution of P_d and of $|E_z|^2$, which can be measured by a survey meter in a line parallel to the array at the distance ρ from the antenna axis, we could use (4) and (6) to plot the distribution of P_d at various distances from the array. This approach does not give the direction of the power flow in the near field, where the main beam and the sidelobes of the antenna are not formed yet. Consider the equation

$$\int_{-\infty}^{+\infty} E_z(\rho, z) H_\phi^*(\rho, z)\, dz = \int_{-\infty}^{+\infty} \tilde{E}_z(\rho, u)\tilde{H}_\phi^*(\rho, u)\, du \tag{7}$$

which is Parseval's formula involving the Fourier Transforms of $E_z(\rho, z)$ and $H_\phi(\rho, z)$, whose expressions are provided in Appendix A. Since ρ is a constant, the analysis of the spectral content of the integrand should give information about the distribution of P_d and its contribution to the radiated power in terms of cylindrical waves propagating outward from the antenna axis. From (4A) and (6A) of Appendix A, the Parseval's integrand is

$$\begin{aligned}\tilde{E}_z(\rho, u)\tilde{H}_\phi^*(\rho, u) = &\frac{\eta}{2\pi}\frac{|I|^2}{\pi^2}\frac{-j\beta}{\sqrt{u^2-\beta^2}}\cos^2(uh) \\ &\cdot K_0\left[\rho\sqrt{u^2-\beta^2}\right] K_1\left[\rho\sqrt{u^2-\beta^2}\right] \\ &\cdot\left[\frac{\sin\frac{up}{2}(2N+1)}{\sin\frac{up}{2}}\right]^2.\end{aligned} \tag{8}$$

Clearly, for $|u| > \beta$ there is no contribution to the $\mathrm{Re}\{E_z H_\phi^*\}$. The spectrum in the visible region $|u| < \beta$ is mostly significant around the saddle point $u = \beta \sin\theta$, with the angle θ defined in Fig. 1. Since we are interested only in the real part of (8), it is clear that the largest contribution comes from $u \approx 0$ provided $p < \lambda$, so no grating lobe contribution must be considered. Moreover, being $\cos^2(\beta h) = 0$, contributions close to the branch cut are negligible. It is interesting to note that an "array factor" is present in (8) for all radial distances. Already for $\rho > \lambda/2$ and $u \approx 0$, the modified Bessel functions can be expanded asymptotically using the formula $K_n(\zeta) \approx \sqrt{\pi/2\zeta}\, e^{-\zeta}$ [13]. In addition, for $N > 0$ the combination of sinusoidal functions in (8) has the maximum value around $u \approx 0$. The main contribution to the real part of the integral (7), coming from the "main lobe" of (8), can be expressed as

$$\begin{aligned}&\mathrm{Re}\int_{-\infty}^{+\infty} \tfrac{1}{2}\tilde{E}_z(\rho, u)\tilde{H}_\phi^*(\rho, u)\, du \\ &\quad\approx \frac{1}{2}\frac{\eta|I|^2}{(2\pi)^2}\frac{1}{\beta\rho}\int_{-u_N}^{+_N}\frac{\sin^2\left[\frac{up}{2}(2N+1)\right]}{\left(\frac{up}{2}\right)^2}\, du\end{aligned} \tag{9}$$

where $u_N \approx \pi/L$. The spectral content of (9) shows that the power flow is relatively uniform over the array because of the cylindrical symmetry of the contributing waves. The integral at right-hand side of (9), corresponding to the "main lobe" of the array factor, gives $\alpha(2N+1)(2\pi/p)$, with $\alpha = (2/\pi)\mathrm{Si}(2\pi) \approx 0.9$, where the *integral sine* function is employed since $\int_0^\pi (\sin x/x)^2\, dx = \int_0^{2\pi}(\sin x/x)\, dx = \mathrm{Si}(2\pi) \approx 1.418$. In conclusion, we have

$$\begin{aligned}&\mathrm{Re}\int_{-\infty}^{+\infty} \tfrac{1}{2} E_z(\rho, z) H_\phi^*(\rho, z)\, dz \\ &\quad\approx \frac{\eta|I|^2}{4\pi}\frac{\alpha(2N+1)}{\beta\rho p} \\ &\quad\approx \alpha\frac{P_{\mathrm{rad}}}{2\pi\rho}\end{aligned} \tag{10}$$

having assumed that the power radiated by the antenna is approximately $(\eta/4\pi)|I|^2(2N+1)$ and that $\beta p \approx 2\pi$. Equation (10) is analogous to (3), and it states that most of the real power flow is contributed by a group of cylindrical waves departing the axis in a narrow angular region near the antenna broadside. The rest of the waves outside this conical region contribute essentially to sidelobes or energy storage. It is of interest to evaluate the decay of the power density (averaged over the array height) near the antenna in the broadside direction for $\rho \geq \lambda/2$.

B. Average Power Density Falloff Versus Distance

The average power density decay versus distance is of interest because it can be expected to be among the parameters of significance for the exposure of humans in the near field of array antennas. In the cylindrical coordinate system, the average power density over the height of the array can be defined as

$$\overline{P}_d(\rho; L) = \frac{1}{2L}\int_{-L}^{L}\mathrm{Re}\left\{\frac{1}{2}E_z(\rho, z)H_\phi^*(\rho, z)\right\} dz. \tag{11}$$

In Fig. 2, this quantity is numerically computed by substituting (4) and (6) in (11) for a nine-element array and used to determine the power intercepted by the cylindrical surface. Though the behavior of $\mathrm{Re}\{E_z(\rho, z)H_\phi^*(\rho, z)\}$ is rather complicated in proximity of the array, the power intercepted has a well-behaved decay with ρ that corresponds to a cylindrical propagation in the near region, which eventually becomes spherical in the far field. In the following, we want to show that this property applies in general to this kind of radiators, as it will be used to determine extremely simple formulas for the estimation of the exposure.

Using the Fourier transform of the magnetic field (4A), we obtain

$$\overline{P}_d(\rho; L) = \mathrm{Re}\left\{\tfrac{1}{2}\int_{-\infty}^{+\infty}\tilde{H}_\phi^*(\rho, u)\tilde{E}_z(\rho, u; L)\, du\right\} \tag{12}$$

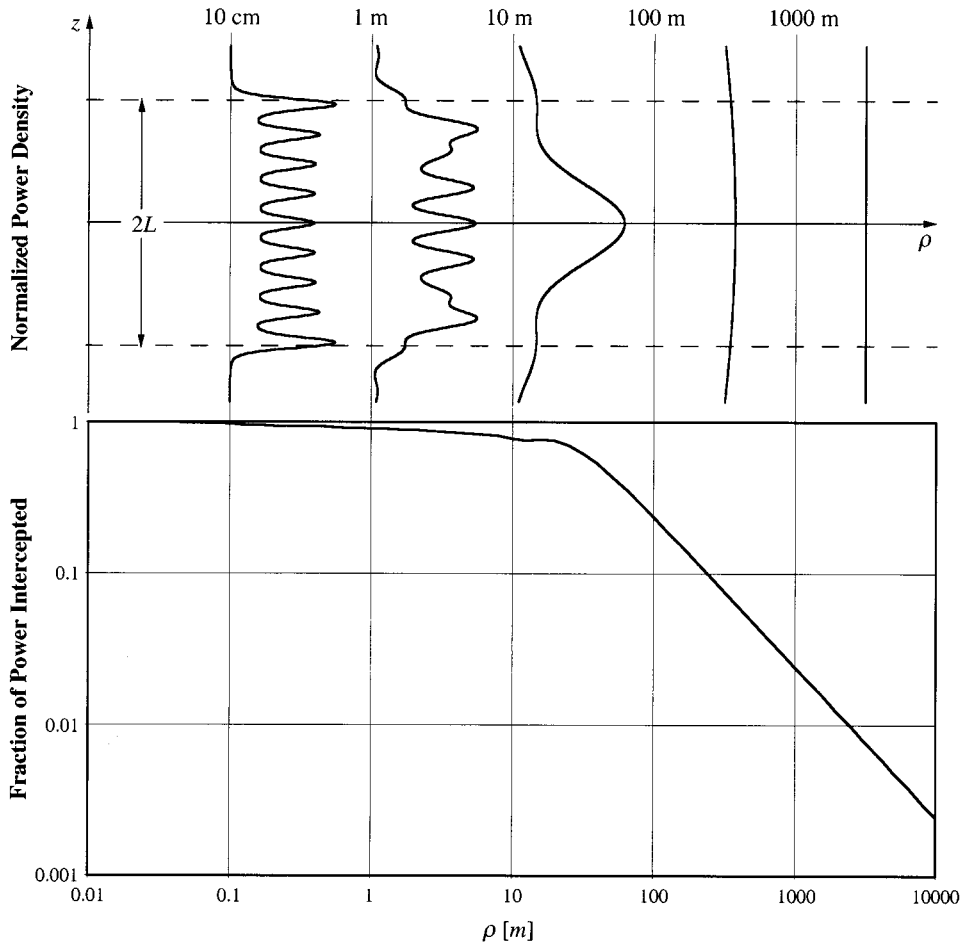

Fig. 2. Normalized power intercepted by the cylindrical surface versus distance. The collinear array is formed by nine half-wave dipoles operating at 900 MHz, separated by $p = \lambda$. The profile of the local power density along a vertical line belonging to the intercepting cylindrical surface is shown at different distances from the array.

where

$$\tilde{E}_z(\rho, u; L) = \frac{1}{2L}\frac{1}{\sqrt{2\pi}}\int_{-L}^{L} E_z(\rho, z)\, e^{juz}\, dz \tag{13}$$

is the partial Fourier transform of the z component of the electric field, which by using (6) becomes

$$\begin{aligned}\tilde{E}_z(\rho, u; L) &= -\frac{j}{\sqrt{2\pi}}\frac{\eta I}{4\pi}\sum_{n=-N}^{N}\left[\frac{1}{2L}\int_{-L}^{L}\frac{e^{-j\beta R_{1,n}}}{R_{1,n}}e^{juz}\,dz\right.\\ &\qquad\left.+\frac{1}{2L}\int_{-L}^{L}\frac{e^{-j\beta R_{2,n}}}{R_{2,n}}e^{juz}\,dz\right].\end{aligned} \tag{14}$$

In (14), we can identify two integral terms, which differ only for the sign of h in (5). Performing the change of variable $z = \rho \sinh t$, the first integral is here rewritten as

$$I_{1,n}(\rho, u; L) = \frac{e^{ju(np+h)}}{2L}\int_{t_{1,n}^{-}}^{t_{1,n}^{+}} e^{-j\rho(\beta\cosh t - u\sinh t)}\,dt \tag{15}$$

with

$$\begin{aligned}t_{1,n}^{-} &= -\sinh^{-1}\left(\frac{L+np+h}{\rho}\right)\\ t_{1,n}^{+} &= \sinh^{-1}\left(\frac{L-np-h}{\rho}\right).\end{aligned} \tag{16}$$

If $\rho \geq 2L$, the hyperbolic functions can be approximated by means of a McLaurin expansion; with the relevant analytical details given in Appendix B, the partial FT becomes

$$\begin{aligned}\tilde{E}_z(\rho, u; L) &= -\frac{1}{\sqrt{2\pi}}\, j\,\frac{\eta I}{4\pi}\, e^{-j\beta\rho}\, e^{ju^2(\rho/2\beta)}\sqrt{\frac{\pi}{\beta\rho}}\\ &\cdot\left[\sum_{n=-N}^{N}\frac{e^{ju(np+h)}}{2L}\left\{\left[C(-x_{1,n}^{-}) + C(x_{1,n}^{+})\right]\right.\right.\\ &\quad\left. -j\left[S(-x_{1,n}^{-}) + S(x_{1,n}^{+})\right]\right\}\\ &\quad+\sum_{n=-N}^{N}\frac{e^{ju(np-h)}}{2L}\left\{\left[C(-x_{2,n}^{-}) + C(x_{2,n}^{+})\right]\right.\\ &\quad\left.\left. -j\left[S(-x_{2,n}^{-}) + S(x_{2,n}^{+})\right]\right\}\right]\end{aligned} \tag{17}$$

where the arguments of the Fresnel integrals $C(\cdot)$, $S(\cdot)$ are

$$x_{1,n}^{\pm} = \sqrt{\frac{\beta}{\pi\rho}}\,(\pm L - np - h) - u\sqrt{\frac{\rho}{\pi\beta}} \tag{18a}$$

$$x_{2,n}^{\pm} = \sqrt{\frac{\beta}{\pi\rho}}\,(\pm L - np + h) - u\sqrt{\frac{\rho}{\pi\beta}}. \tag{18b}$$

Equation (17) is very important, since it will allow us to determine the character of the average power density decay versus distance. In fact, (17) clearly features a cylindrical term modulated by a summation of Fresnel integrals. The character of the combination of these integrals may be better understood after expressing them in terms of the following auxiliary functions [13]:

$$f(x) = \left[\frac{1}{2} - S(x)\right]\cos\left(\frac{\pi}{2}x^2\right) - \left[\frac{1}{2} - C(x)\right]\sin\left(\frac{\pi}{2}x^2\right) \tag{19}$$

$$g(x) = \left[\frac{1}{2} - C(x)\right]\cos\left(\frac{\pi}{2}x^2\right) + \left[\frac{1}{2} - S(x)\right]\sin\left(\frac{\pi}{2}x^2\right) \tag{20}$$

which exhibit a very smooth behavior, shown in Fig. 3, that is well approximated by means of rational functions [13]. Moreover, the following relationships involving their derivatives hold: $f'(x) = -\pi\, x\, g(x)$, $g'(x) = \pi\, x\, f(x) - 1$. These auxiliary functions can be substituted in (17), yielding

$$\begin{aligned}
&\tilde{E}_z(\rho, u; L)\\
&= -\frac{(1+j)}{2L\sqrt{2\pi}}\,\frac{\eta I}{2\pi}\,e^{-j\beta\rho}\,e^{ju^2(\rho/2\beta)}\sqrt{\frac{\pi}{\beta\rho}}\,\cos(uh)\\
&\quad\cdot\left[\frac{\sin\frac{up}{2}(2N+1)}{\sin\frac{up}{2}}\right] - \frac{j}{2L\sqrt{2\pi}}\,\frac{\eta I}{4\pi}\,e^{-j\beta\rho}\\
&\quad\cdot\sqrt{\frac{\pi}{\beta\rho}}\left[e^{-juL}\sum_{n=-N}^{N}\Big\{\left[jf(-x_{1,n}^{-}) - g(-x_{1,n}^{-})\right]\right.\\
&\qquad\cdot e^{-j(\beta/2\rho)(L+np+h)^2} + \left[jf(-x_{2,n}^{-}) - g(-x_{2,n}^{-})\right]\\
&\qquad\cdot e^{-j(\beta/2\rho)(L+np-h)^2}\Big\} + e^{juL}\sum_{n=-N}^{N}\\
&\qquad\cdot\Big\{\left[jf(x_{1,n}^{+}) - g(x_{1,n}^{+})\right]\,e^{-j(\beta/2\rho)(L-np-h)^2}\\
&\qquad\left.+\left[jf(x_{2,n}^{+}) - g(x_{2,n}^{+})\right]\,e^{-j(\beta/2\rho)(L-np+h)^2}\Big\}\right].
\end{aligned} \tag{21}$$

It is interesting to note that the first term in (21), featuring a cylindrical decay, is almost identical to the Fourier transform (6A) employed in (9), the only difference being a factor proportional to u^4 and higher powers of u in the exponential term, which has a negligible impact over the main lobe of the array factor. This result further reinforces the notion that hardly any energy escapes through the sidelobes for $\rho \le 2L$. The character of the second term in (21) can be established by looking at

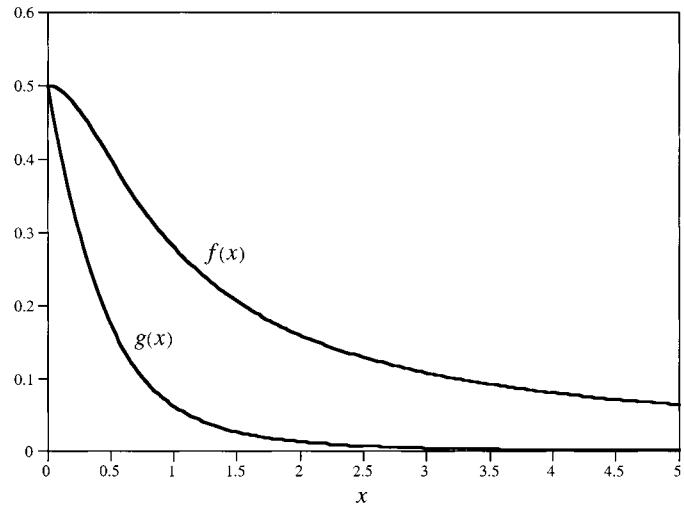

Fig. 3. Behavior of the auxiliary functions used to express the Fresnel integrals. As the distance from the array is increased, their arguments tend to vanish.

the behavior of the auxiliary functions f, g as their arguments $x_{1,n}^{\pm}$, $x_{2,n}^{\pm}$ change with ρ. At large radial distances, we can limit our attention to spectral waves propagating in the broadside direction, whose spectrum is sampled at the saddle point $u = \beta\sin\theta = \beta z/\sqrt{\rho^2 + z^2}$. In this case, $u \propto 1/\rho$, provided $-L \le z \le L$, and therefore the arguments of the auxiliary function tend to vanish, which allows us to approximate these functions by means of a first-order McLaurin expansion $jf(x) - g(x) \approx (j-1)/2 + x$. Upon neglecting higher order contributions ($\rho^{-\nu}$, $\nu > 1$), it can be seen that the second term in (21) splits in a new cylindrical contribution and a spherical contribution. The former asymptotically eliminates the preexistent cylindrical term in (21), so that the latter eventually dictates the far-field character of the electric field

$$\tilde{E}_z(\rho, u; L) \approx -j\,\frac{(2N+1)}{\sqrt{2\pi}}\,\frac{\eta I}{2\pi\rho}\,e^{-j\beta\rho}\cos(uL). \tag{22}$$

As we get closer to the antenna, the arguments of the auxiliary functions increase, i.e., these functions are no longer sampled around their maximum, instead they rather tend to vanish. Consequently they no longer suppress the cylindrical term in (21). What happens, indeed, is that the auxiliary functions are modulated in a somewhat complicated fashion by the exponential factors in (21). It can be seen in Fig. 2 that there is a transition region in the near field where the average power density exhibits a slight oscillatory behavior, which can be associated with the loss of energy through the various sidelobes that gradually escape the intercepting cylinder of Fig. 1.

The previous results can be used to determine the character of the average power density given in (12). Already at a short distance away from the array ($\rho > \lambda/2$), its expanded expression in (23), given at the bottom of the next page, shows a $\rho^{-1/2}$ factor that, when combined with the initial $\rho^{-1/2}$ decay of the partial FT (21), establishes the cylindrical character of the average power density in the vicinity of the collinear array. As we move away from the antenna, the partial FT (22) becomes representative of the actual behavior of the electric field. When substituted in (23), the phase term of the integrand takes the exponential

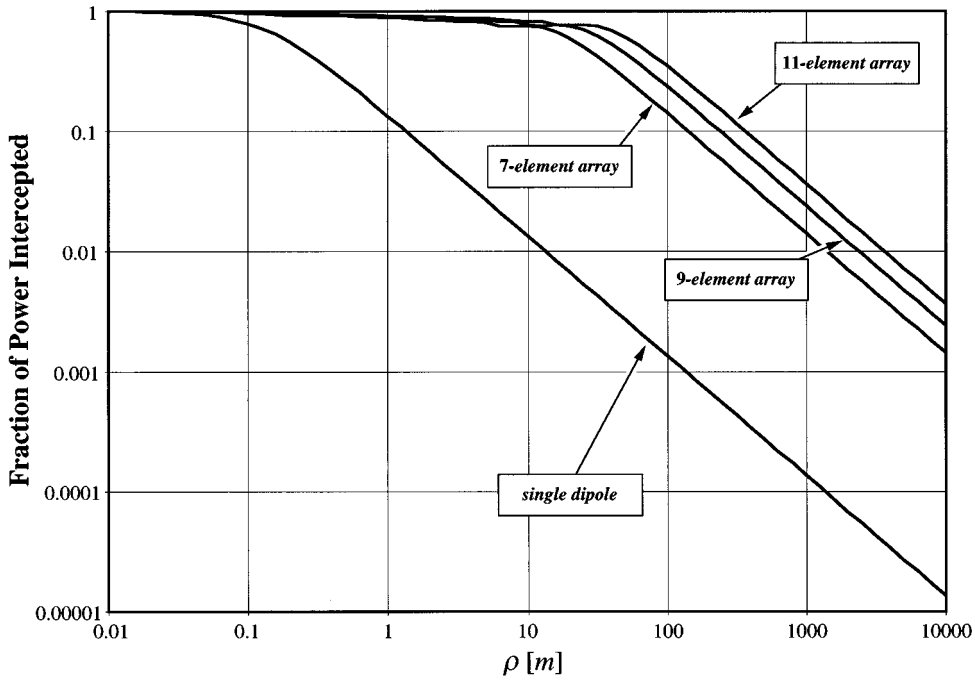

Fig. 4. Computed decay versus distance of the power intercepted by the lateral cylindrical surface for a single half-wave dipole operating at 900 MHz and for 7-, 9-, and 11-elements collinear arrays ($p = \lambda$). The increasing size and gain push the point where the propagating field assumes the spherical character farther away from the array.

form: $\exp(j\rho\sqrt{\beta^2 - u^2} - j\rho\beta) \approx \exp(-j\rho u^2/2\beta)$. The remaining portion of the integrand (which is an even function of u) is weighted by two "spectral windows": the array factor and the just-mentioned exponential term (whose main contribution to the integral is its cosine $\cos[\rho u^2/2\beta]$). The former establishes the significant contribution to the integral in (23) in the region closer to the array, while the latter away from it. We may define a break point where the main lobe of the array factor equals the main lobe of $\cos[\rho u^2/2\beta]$, the resulting condition being

$$u = \sqrt{\frac{\pi\beta}{\overline{\rho}}} = \frac{2\pi}{p(2N+1)}; \quad \overline{\rho} = \kappa(2N+1)L, \quad \kappa = \frac{p}{\lambda}. \tag{24}$$

When $\kappa = 1$, then $\overline{\rho} = 2L^2/\lambda = (2L)^2/2\lambda$. The distance $\overline{\rho}$ happens to coincide with the point where the main lobe of the array is completely inside the intercepting cylindrical surface. In conclusion, for $\rho < \overline{\rho}$ the significant "windowing function" is $\sin[up(2N+1)/2]/\sin[up/2]$, which is independent of ρ, and therefore the ρ dependence of (23) is essentially cylindrical in the near region. Beyond $\overline{\rho}$, the integral contribution is weighted by the ρ-dependent "cosine window" combined with the ρ^{-1} far-field character of $\tilde{E}_z(\rho, u; L)$ and the $\rho^{-1/2}$ factor in (23). The area under the main lobe of $\cos[\rho u^2/2\beta]$ is clearly proportional to $\rho^{-1/2}$

$$\begin{aligned} A(\rho) &= 2 \cdot \int_0^{\sqrt{\pi\beta/\rho}} \cos\left(\rho\,\frac{u^2}{2\beta}\right) du \\ &= \sqrt{\frac{\pi\beta}{\rho}} \cdot 2\int_0^1 \cos\left(\frac{\pi}{2}x^2\right) dx \\ &\cong \frac{6.93}{\sqrt{\rho\lambda}} \end{aligned} \tag{25}$$

which finally gives the spherical character of the average power density in the far field. In Fig. 4, the normalized power fall-off is shown in the case of uniformly fed 7-, 9-, and 11-element collinear arrays, as well as for a single half-wave dipole. The increasing gain of the array as more elements are added moves farther away the break point where the spherical character of the propagating field is established. Up to that point, the share of power escaping through the top and bottom surfaces of the cylinder is substantially limited to that contained in the array antenna sidelobes.

We can now discuss the meaning of near E-field measurements close to a collinear array along the axis of the antenna.

$$\overline{P}_d(\rho; L) = \frac{\mathrm{Re}\left\{\displaystyle\int_{-\infty}^{+\infty} \frac{\beta I^* \cos(uh)}{\sqrt{(-j\beta)^2 + u^2}}\, \frac{e^{j\rho\sqrt{\beta^2-u^2}}}{\sqrt[4]{\beta^2 - u^2}} \left[\frac{\sin\dfrac{up}{2}(2N+1)}{\sin\dfrac{up}{2}}\right] \tilde{E}_z(\rho, u; L)\, du\right\}}{4\pi\sqrt{\rho}} \tag{23}$$

III. Significance of Electric Energy Density Measurements Near Base Stations

The survey measurements of the exposure of humans near collinear arrays are often performed by scanning a E-field sensing probe along a line parallel to the antenna axis at a constant radial distance from the radiating structures. Usually, these probes have a square-law response, giving a reading proportional to $|\boldsymbol{E}|^2$ if the probe sensor is isotropic. The display of such metering devices is calibrated in mW/cm^2 (some more appropriately give the results in V^2/m^2) and the measurement is often taken as an evaluation of the power density of the exposure, even though $|\boldsymbol{E}|^2$ may have little or no relation to the real power flow. Very close to the array, but at least a wavelength away to avoid contributions from the strong reactive fields surrounding the array elements, we have $|E_\rho(\rho, z)| \ll |E_z(\rho, z)|$. Therefore, the power flow density is

$$\begin{aligned}\mathrm{Re}\{\tfrac{1}{2}\boldsymbol{E}\times\boldsymbol{H}^*\cdot\hat{\boldsymbol{r}}\} &\approx \mathrm{Re}\{\tfrac{1}{2}E_z H_\phi^*\}\\ &\sim \frac{1}{2\eta}|E_z|^2\end{aligned} \tag{26}$$

since for cylindrical waves radiated close to broadside $E_z \approx \eta H_\phi$ [this can be verified taking the ratio between the Fourier transforms (6A) and (4A) as the significant contribution to the spectral propagating waves comes from around $u \approx 0$].

The different phase delays experienced by the electromagnetic waves originating from each radiator produce a rather oscillating behavior of the vertical distribution of E_z close to the antenna, as shown in Fig. 2. However, the average the power density over the height of the antenna, computed using (26) after sampling E_z, has a smooth decay. So it is possible to measure real power density in an average sense if an E-field meter is used at any distance from the array greater than $\approx \lambda/2$. One interesting outcome of the considerations made in Section II-A is that the sidelobes contain less than 10% of the antenna radiated power, although it may be very difficult to define the sidelobes in the immediate vicinity of the array because of their shifting directions. The first sidelobe, at some locations, may shift in and out of the main lobe, depending on the array size and distance; some sidelobes may coalesce. The only statement that can be made about the measurement of $|\boldsymbol{E}|^2$ in the immediate vicinity of the array is that it tends to slightly overstate the local power density taken as $|E_z|^2/2\eta$. The reason for the overestimation of the power is that $(|E_\rho|^2+|E_z|^2)/2\eta$ gives approximately (if the wave impedance is about $377\,\Omega$) the magnitude of the Poynting vector rather than the real part of the Poynting vector at a given point.

At sufficient distance from the array, if the E-field probe still gives any readings, a local power density measurement can be performed by measuring only the electric field component which is orthogonal to the direction of propagation. This measurement is by no means trivial, given the sensitivity of most probes to their orientation with respect to the incident E field. The only measurement of significance is the one of the average of $|E_z|^2$ over the length of the array because it is related to the average power density as discussed in Section II-A. It is difficult to perform such measurement with isotropic field probes, because they respond to $|\boldsymbol{E}|^2$. A single axis or a two-axes E-field sensor is more suitable for the measurement of $|E_z|^2$ than the isotropic probes, which are normally used for survey purpose.

Evidently, it would be a convenient result to have at our disposal a simple way to predict the average power density at any distance from the array with a precision comparable to the measurement uncertainty. In the next section, some simple formulas are derived based on the theory presented in Section II.

IV. Formulas for the Prediction of the Average Exposure

A. Collinear Arrays

We will use the results of Section II as they allow us to determine a simple prediction formula for the average power flow through the intercepting cylindrical surface of height $2L$. Simple geometrical considerations lead us to define a distance where the character of the average power density changes from prevalently cylindrical to prevalently spherical. The power intercepted by the cylindrical surface at a distance ρ, in the far field, is

$$\begin{aligned}P_{\mathrm{sph}}(\rho;\,L) &= \frac{P_{\mathrm{rad}}G_A}{4\pi\rho^2}\cdot 2L\cdot 2\pi\rho\\ &= \frac{P_{\mathrm{rad}}G_A}{\rho}\cdot L \le P_{\mathrm{rad}} \quad\Rightarrow\quad \rho \ge G_A L\end{aligned} \tag{27}$$

where G_A is the collinear array broadside gain, whereas in the near region, where the field propagation is prevalently cylindrical, the intercepted power is $P_{\mathrm{cyl}}(\rho;\,L) = P_{\mathrm{rad}}$. The condition $P_{\mathrm{cyl}}(\rho;\,L) \le P_{\mathrm{sph}}(\rho;\,L)$ can be valid only for $\rho \le G_A L$. From these considerations, the distance is naturally found as $\rho_0 = G_A L$. The actual behavior of the intercepted power versus distance, computed as described in Section II, is well approximated by the following:

$$P_{\mathrm{int}}(\rho;\,L) = \frac{P_{\mathrm{rad}}}{\sqrt{1+(\rho/\rho_0)^2}}, \qquad \rho_0 = G_A L. \tag{28}$$

As shown in Fig. 5, this formula approximates within a few tenths of a decibel the computed behavior. Equation (28) provides an accurate and extremely simple way to establish the exposure levels in the immediate vicinity of base-station antennas. In fact, it features a slight overestimate of the resulting average power density, which can be expressed as

$$\overline{P}_d(\rho;\,L) = \frac{P_{\mathrm{rad}}}{2L\cdot 2\pi\rho\,\sqrt{1+(\rho/\rho_0)^2}}, \qquad \rho_0 = G_A L. \tag{29}$$

This overestimation makes the use of (29) even more convenient for exposure assessment because parameters such as the array gain and dimension should be readily available to survey personnel.

The proposed prediction formulas remain valid even when the illumination of the array is tapered in order to reduce the sidelobe levels. In fact, in this case the gain is reduced as well due to the shorter "effective length" of the array, and the beamwidth is increased, meaning that the propagating field assumes the spherical character earlier than in the case of uniform illumination. Moreover, the oscillatory behavior experienced in the transition region where the character of the field goes from prevalently

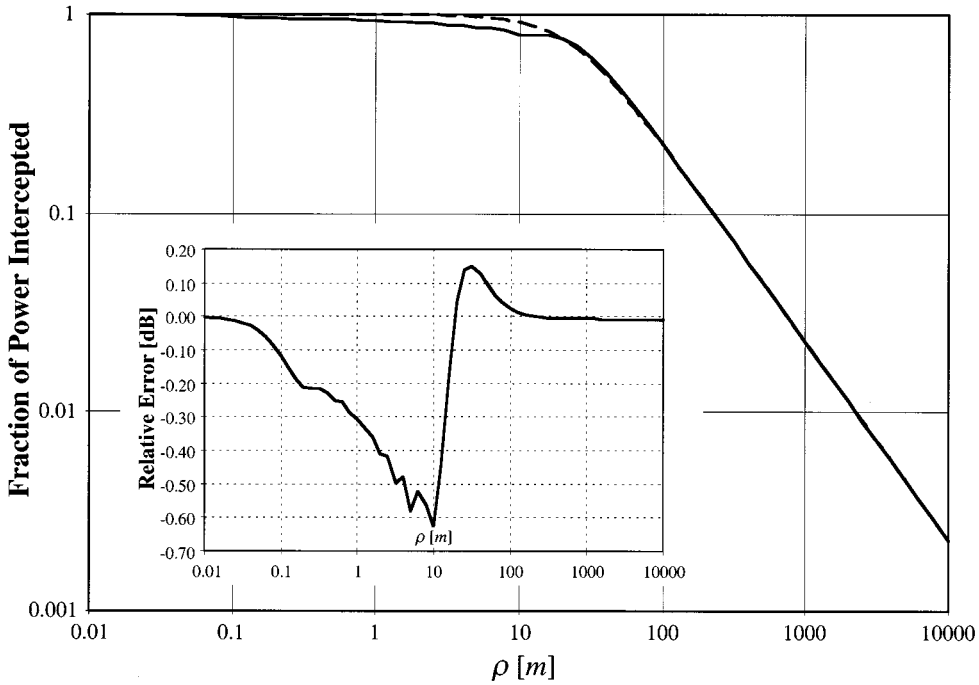

Fig. 5. Normalized power intercepted by the lateral cylindrical surface versus distance for a uniformly fed nine-element collinear array operating at 900 MHz ($p = \lambda$): comparison between the computed behavior and the prediction formula (28).

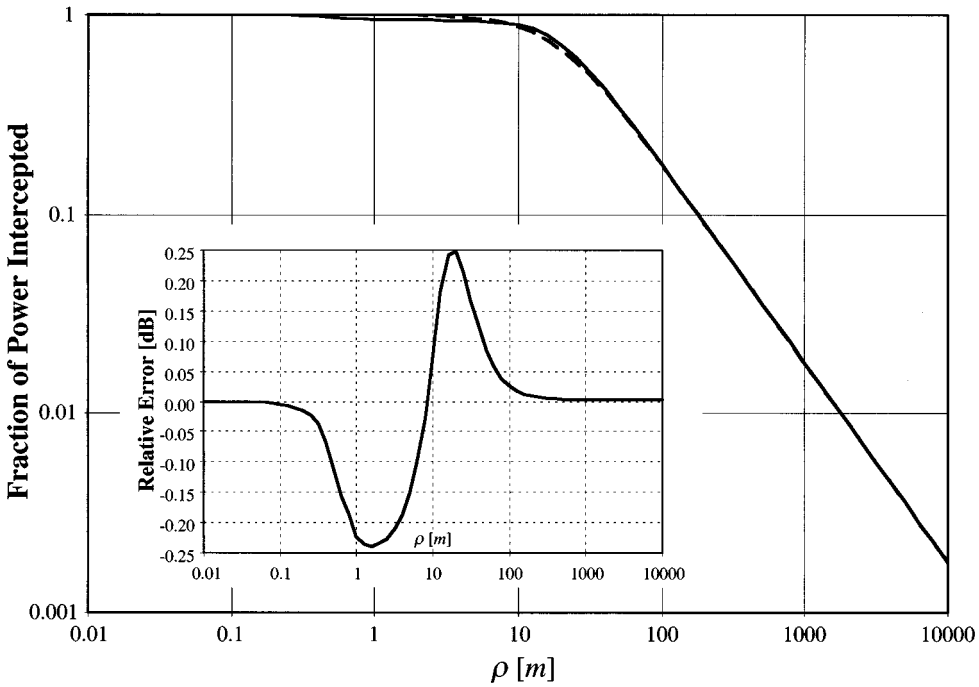

Fig. 6. Normalized power intercepted by the lateral cylindrical surface versus distance for a *non*uniformly fed nine-element collinear array operating at 900 MHz ($p = \lambda$): comparison between the computed behavior and the prediction formula (28). The feed-point currents follow a cosine square profile; their amplitudes are given in Table I.

cylindrical to spherical is smoothed, given the reduced amount of energy escaping through the sidelobes. Both these features are shown in Fig. 6, where the same nine-element collinear array previously considered is fed now using a cosine square taper for the feed-point current amplitudes. We clearly see how the smoother power decay results in a closer agreement with the prediction formula (28). This result justifies neglecting the mutual coupling between array elements. As discussed in Section II, the main effect of mutual coupling is to increase the feed-point currents. This effect is less pronounced on the outermost elements, since they adjoin with only one other element. Indeed, the end result is that the symmetry of the illumination is preserved, as long as the feeding network operates properly, and the above considerations on the character of the field hold.

TABLE I
PROFILE OF THE FEEDING CURRENTS OF A NINE-ELEMENT COLLINEAR ARRAY

ELEMENT #	HEIGHT	FEED-POINT CURRENT
1	$z = 4\lambda$	$0.096\angle 0°$ A
2	$z = 3\lambda$	$0.346\angle 0°$ A
3	$z = 2\lambda$	$0.655\angle 0°$ A
4	$z = \lambda$	$0.905\angle 0°$ A
5	$z = 0$	$1.0\angle 0°$ A
6	$z = -\lambda$	$0.905\angle 0°$ A
7	$z = -2\lambda$	$0.655\angle 0°$ A
8	$z = -3\lambda$	$0.346\angle 0°$ A
9	$z = -4\lambda$	$0.096\angle 0°$ A

Measurements have been performed to verify the behavior of the average power density in the vicinity of some practical arrays. A *Celwave PD1610* two-element collinear dipole array operating at 870 MHz was measured using a *Narda* 8621D isotropic E-field probe, with readings in V/m. The conversion to mW/cm^2 is meaningful provided that the reactive E-field is negligible. The results plotted in Fig. 7 exhibit a good agreement with the prediction formula, as they show the initial cylindrical character of the propagating field.

B. Other Directive Antennas

We take into account the situation where the radiators of the basestation antenna are backed by reflectors in order to direct RF energy in a specific sector. We considered a right corner reflector antenna (the radiator being a half-wave dipole), model DB495-C by DECIBEL PRODUCTS, operating at 940 MHz, and estimated the average (over the height of the reflector) power density as the distance from the antenna was increased. Its behavior, shown in Fig. 8, was then fitted using a variation of formula (29), where the substantial confinement of the electromagnetic radiation to the right angle sector was accounted for by substituting the reflector's angle ($\pi/2$) for the 2π factor originated from the cylindrical symmetry. In the case of a reflector having a semiaperture angle $\gamma\,(\leq 90°)$, (29) can be generalized as follows:

$$\overline{P}_d(\rho, |\phi| < \gamma; L) = \frac{P_{\rm rad}}{4\gamma L \cdot \rho\sqrt{1+(\rho/\rho_0)^2}}, \qquad \rho_0 = \frac{\gamma}{\pi} G_A L \tag{30}$$

which maintains the simplicity of (29), but could result in an underestimation in directions close to $\phi \approx 0$, an inconvenience for survey purposes because the reflector narrows the beam in both elevation and azimuth, thus increasing the antenna gain. In fact, the far-field radiation pattern of the corner reflector antenna has been measured in the Motorola's anechoic facility in Fort Lauderdale, FL; its resulting gain is about 10 dBi. Assuming a Gaussian ϕ dependence for the power density, which also has been verified from the radiation pattern, and neglecting edge diffraction (the power density at $|\phi| = 45°$ being at least 10 dB below the peak), (30) can be refined as follows:

$$\overline{P}_d(\rho, |\phi| < \gamma; L) = \frac{P_{\rm rad}}{4\gamma L \cdot \rho\sqrt{1+(\rho/\rho_0)^2}} \left[\sqrt{\frac{8}{\pi}}\, e^{-2(\phi/\gamma)^2}\right], \qquad \rho_0 = \frac{\gamma}{\sqrt{8\pi}} G_A L \tag{31}$$

where the factor $\sqrt{8/\pi} \approx 1.6$ comes from enforcing that the entire power radiated is confined to the sector $|\phi| < \gamma$. Neglecting this constraint, this factor could be directly included in the formula (30) to provide a slight overestimation in directions away from $\phi \approx 0$. There is no real need to consider directions belonging to the complementary sector where diffracted fields propagate. Typically, only in directions around $|\phi| \approx 180°$ the diffracted field contributions combine constructively to form the backlobe of the antenna, having very little power associated with it.

Finally, it is interesting to notice that substantially similar behavior can be expected from a Yagi–Uda array, such as the AEA CUY4-10RT ten-element antenna operating at 865 MHz that was measured. The relevant results are given in Fig. 9. In this case, it was found that close to the antenna the average power density decay in the end-fire direction can be predicted readily as

$$\overline{P}_d(\rho, \phi \approx 0; h_d) = \frac{P_{\rm rad}}{2\pi h_d \rho} \tag{32}$$

where the confinement of the radiation beam and the consequent high gain result from the use of the director elements length h_d instead of the (larger) effective length of the antenna, rather than a reduction of the aperture angle, which remains 2π in this formula.

C. Partial Exposure

A straightforward application of the prediction formulas may overestimate the actual exposure since the person may not be entirely contained in the intercepting cylinder [as defined in Section II-B (see Fig. 1)], especially in close proximity of large arrays. The value predicted by the formulas can be adjusted to reflect the actual exposure by means of a scaling factor that accounts for the partial penetration of the exposed human body in the cylinder

$$\overline{P}_d(\rho; L; T, H) = \overline{P}_d(\rho; L) \times \left(\frac{T}{H}\right), \qquad \rho \ll \rho_0 \tag{33}$$

where H is the height of the person standing parallel in front of the antenna and T the intercepted portion. Should the array be slightly tilted, as happens on rooftop installation in high buildings, the closest distance may be used in the formulas. Equation (33) may only be applied if the person stands at a distance from the array where the propagation is still substantially cylindrical in character and there is a sharp discontinuity between the illuminated and the shaded regions of the exposed body, hence, the limitation established in (33).

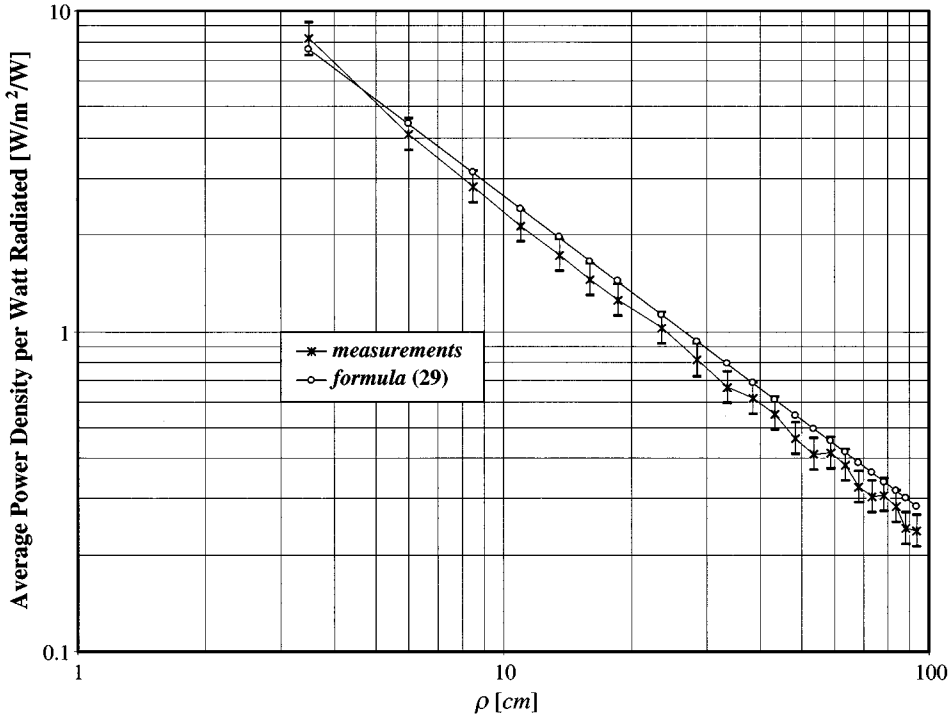

Fig. 7. Average power density in the vicinity of the *Celwave PD1610* two-element array operating at 870 MHz, measured using the *Narda* 8621D probe. A good agreement with the prediction formula (29) is observed.

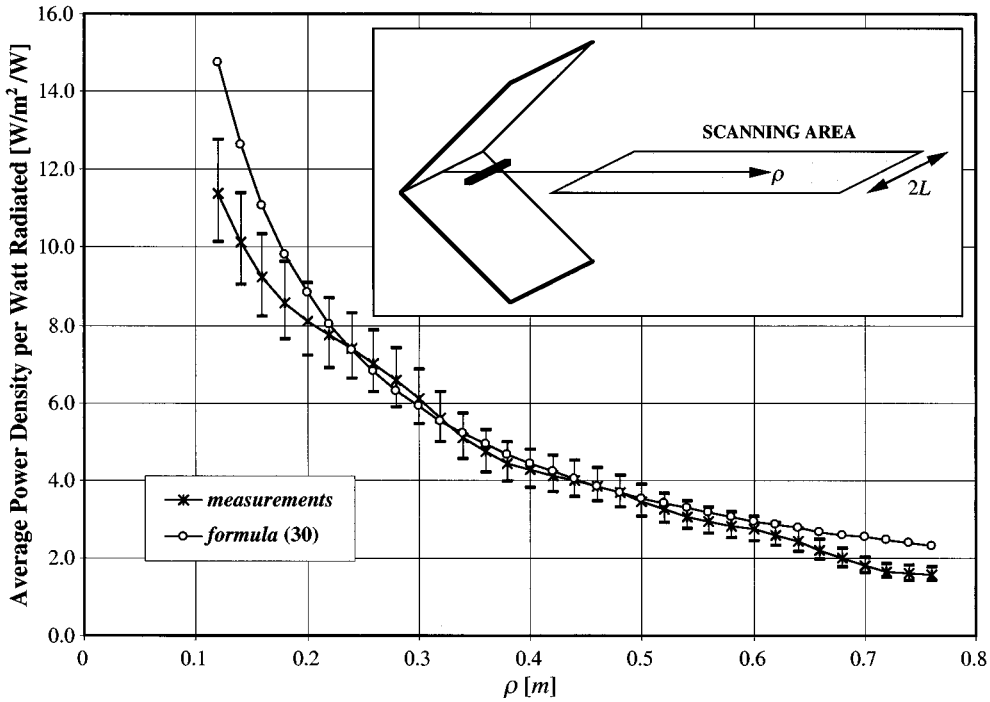

Fig. 8. Average power density in the vicinity of the DECIBEL DB495-C right corner reflector antenna operating at 940 MHz, measured using the DASY2 robotic system. The distance from the antenna is measured from the reflector's corner. The average power density falloff is well approximated by (30).

V. Final Remarks

The human exposure to electromagnetic radiation emanating from cellular base stations has raised concern, involving both the general population and personnel engaged in routine maintenance work. Whereas the exposure to reactive fields in the close proximity of radiating sources ($\rho < \lambda/2$), where the tight coupling with the human body likely affects antenna performance, can be only estimated with SAR measurements (as in the case of cellular telephones [2], [3]), the exposure to this kind of radiators takes place almost exclusively in nonreactive field, and the relevant exposure limits are defined with respect of the incident

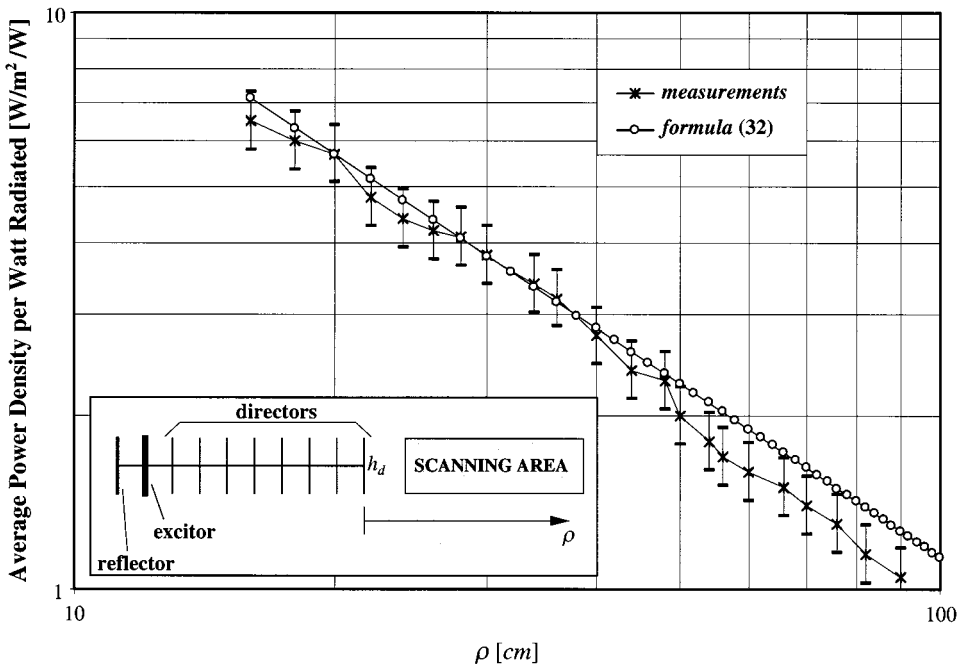

Fig. 9. Average power density in the vicinity of the AEA CUY4-10RT ten-element Yagi-Uda antenna operating at 865 MHz, measured using a *Narda* 8621D probe. In this case, the distance from the array is taken from the last director. The average power density decay has a definite cylindrical character, which is approximated by (32).

power density averaged over the whole human body, which is usually measured along lines parallel to the array axis. In this paper, we show that this quantity has a predictable behavior, which can be estimated by means of simple and accurate formulas whose parameters are readily available. In fact, in the case of a collinear array, which is representative of most base-station antennas, even if reflectors or other type of elemental radiators are employed, the average power density decay in the vicinity of the antenna has a definite cylindrical character, which gradually converts to the eventual spherical far-field behavior.

The result is remarkably simple and can be used to check survey results, if the measurement samples are averaged over a height equal at least to the half length of the array. The suggested approach can be adopted by maintenance personnel to verify the compliance to safety limits, even in conditions of very close proximity to base-station antennas, where the highest exposure levels can be expected in most cellular phone base installations.

APPENDIX A

Adopting the following Fourier transform definition:

$$\tilde{\psi}(u) = \frac{1}{\sqrt{2\pi}} \int_{-\infty}^{+\infty} \psi(z) e^{juz}\, dz \quad \leftrightarrow$$
$$\psi(z) = \frac{1}{\sqrt{2\pi}} \int_{-\infty}^{+\infty} \tilde{\psi}(u) e^{-juz}\, dz \tag{1A}$$

the FT of $H_\phi(\rho, z)$ can be computed by evaluating the integral

$$\int_{-\infty}^{+\infty} e^{-j\beta\sqrt{\rho^2+(z-np\pm h)^2}}\, e^{juz}\, dz = e^{ju(np\mp h)} \int_{-\infty}^{+\infty} e^{-j\beta\sqrt{\rho^2+z^2}}\, e^{juz}\, dz. \tag{2A}$$

The integral of the right-hand side of (2A) is given by [13]

$$\int_{-\infty}^{+\infty} e^{-j\beta\sqrt{\rho^2+z^2}}\, e^{juz}\, dz = \frac{2j\beta\rho}{\sqrt{(j\beta)^2+u^2}}\, K_1\left[\rho\sqrt{(j\beta)^2+u^2}\right] \tag{3A}$$

where K_1 is a first-order modified Bessel function of the second kind [13]. From (3A), the FT of $H_\phi(\rho, z)$ is found to be

$$\tilde{H}_\phi(\rho, u) = \frac{1}{\sqrt{2\pi}}\, j\, \frac{I}{\pi}\, \frac{j\beta}{\sqrt{(j\beta)^2+u^2}}\, K_1\left[\rho\sqrt{(j\beta)^2+u^2}\right] \cdot \cos(uh) \left[\frac{\sin\frac{up}{2}(2N+1)}{\sin\frac{up}{2}}\right]. \tag{4A}$$

The FT of the electric field components are found substituting (4A) in (6) and using the recurrence formula $xK_n'(x) + nK_n(x) = -xK_{n-1}(x)$ [13], resulting in

$$\tilde{E}_\rho(\rho, u) = ju\, \frac{1}{\sqrt{2\pi}}\, \frac{I}{\pi}\, \frac{j\eta}{\sqrt{(j\beta)^2+u^2}}\, K_1\left[\rho\sqrt{(j\beta)^2+u^2}\right] \cdot \cos(uh) \left[\frac{\sin\frac{up}{2}(2N+1)}{\sin\frac{up}{2}}\right] \tag{5A}$$

$$\tilde{E}_z(\rho, u) = -\frac{j\eta}{\sqrt{2\pi}}\, \frac{I}{\pi}\, K_0\left[\rho\sqrt{(j\beta)^2+u^2}\right] \cdot \cos(uh) \left[\frac{\sin\frac{up}{2}(2N+1)}{\sin\frac{up}{2}}\right] \tag{6A}$$

where $\eta \approx 377\Omega$ is the characteristic impedance of the free space. For $|u| < \beta$ we select the branch $+j\sqrt{\beta^2 - u^2}$, giving

$$K_1\left(j\rho\sqrt{\beta^2-u^2}\right) = \frac{\pi}{2}\,H_1^{(2)}\left(\rho\sqrt{\beta^2-u^2}\right) \tag{7A}$$

$$K_0\left(j\rho\sqrt{\beta^2-u^2}\right) = -j\,\frac{\pi}{2}\,H_0^{(2)}\left(\rho\sqrt{\beta^2-u^2}\right) \tag{8A}$$

where $H_0^{(2)}$ and $H_1^{(2)}$ are second-kind Hankel functions of order 0 and 1, respectively. The near field components have now been expressed in terms of cylindrical rather than spherical waves. Equations (4A)–(6A) show that the waves with $|u| < \beta$ propagate energy away from the source, while the waves with $|u| > \beta$ give rise to evanescent waves that decay exponentially away from the axis of the array and contribute little amplitude to the field even for relatively small values of ρ.

APPENDIX B

For $\rho \geq 2L$, the integration limits in (15) are always confined in $[-1, 1]$. They can be rewritten

$$t_{1,n}^{-} \approx -\frac{L+np+h}{\rho}, \quad t_{1,n}^{+} \approx \frac{L-np-h}{\rho} \tag{1B}$$

so that the hyperbolic functions can be approximated as $\sinh t \approx t$, $\cosh t \approx 1 + t^2/2$, with (15) becoming

$$I_{1,n}(\rho, u; L) = \frac{e^{ju(np+h)}}{2L}\; e^{-j\beta\rho}\; e^{ju^2(\rho/2\beta)} \cdot \int_{t_{1,n}^{-}}^{t_{1,n}^{+}} e^{-j\left(t\sqrt{\beta\rho/2} - u\sqrt{\rho/2\beta}\right)^2}\, dt. \tag{2B}$$

Let us substitute $x = \sqrt{2/\pi}\left(t\sqrt{\beta\rho/2} - u\sqrt{\rho/2\beta}\right)$, thus obtaining

$$I_{1,n}(\rho, u; L) = \frac{e^{ju(np+h)}}{2L}\, e^{ju^2(\rho/2\beta)}\, e^{-j\beta\rho}\sqrt{\frac{\pi}{\beta\rho}} \cdot \{[C(-x_{1,n}^{-}) + C(x_{1,n}^{+})] - j[S(-x_{1,n}^{-}) + S(x_{1,n}^{+})]\} \tag{3B}$$

where

$$C(x) = \int_0^x \cos\left(\frac{\pi}{2}\,w^2\right) dw, \quad S(x) = \int_0^x \sin\left(\frac{\pi}{2}\,w^2\right) dw \tag{4B}$$

are the Fresnel integrals. We can derive a similar expression for the other integral upon changing $h \to -h$

$$I_{2,n}(\rho, u; L) = \frac{e^{ju(np-h)}}{2L}\, e^{ju^2(\rho/2\beta)}\, e^{-j\beta\rho}\sqrt{\frac{\pi}{\beta\rho}} \cdot \{[C(-x_{2,n}^{-}) + C(x_{2,n}^{+})] - j[S(-x_{2,n}^{-}) + S(x_{2,n}^{+})]\}. \tag{5B}$$

ACKNOWLEDGMENT

The authors would like to thank the entire staff at the Motorola Florida Corporate Electromagnetics Research Lab for their support as well as Prof. R. Cicchetti of the University of Rome "La Sapienza," Italy, for his helpful suggestions.

REFERENCES

[1] Q. Balzano, "Safety aspects of portable and mobile communication antenna design," in *Mobile Antenna Systems Handbook*, K. Fujimoto and J. R. James, Eds. Norwood, MA: Artech, 1994.
[2] Q. Balzano, O. Garay, and T. J. Manning, Jr., "Electromagnetic energy exposure of simulated users of portable cellular telephones," *IEEE Trans. Veh. Technol.*, vol. 44, pp. 390–403, Aug. 1995.
[3] T. Schmid, O. Egger, and N. Kuster, "Automated E-field scanning system for dosimetric assessments," *IEEE Trans. Microwave Theory Tech.*, vol. 44, pp. 105–113, Jan. 1996.
[4] *Radio-Frequency Radiation Handbook*, 4 ed., USAF School of Aerospace Medicine, Brooks Air Force Base, TX, 1986.
[5] P. J. Dymbylow and S. M. Mann, "SAR calculations in an anatomically correct model of the head for mobile communication transceivers at 400 MHz and 1.8 GHz," *Phys. Med. Biol.*, vol. 39, pp. 1537–1553, 1994.
[6] O. Gandhi, G. Lazzi, and C. M. Furse, "Electromagnetic absorption in the human head and neck for mobile telephones at 835 and 1900 MHz," *IEEE Trans. Microwave Theory Tech.*, vol. 44, pp. 1884–1897, Oct. 1996.
[7] *Standard for Safety Levels with Respect to Human Exposure to RF Electromagnetic Fields, 3 kHz to 300 GHz*, IEEE Standard C95.1-1999.
[8] "Guideline for limiting exposure to time-varying electric, magnetic, and electromagnetic fields," *Health Phys.*, vol. 74, no. 4, pp. 494–522, Apr. 1998.
[9] *IEEE Recommended Practice for the Measurement of Potentially Hazardous Electromagnetic Fields-RF and Microwaves*, IEEE Standard C95.3-1991.
[10] R. C. Petersen and P. A. Testagrossa, "Radio- frequency electromagnetic fields associated with cellular-radio cell-site antennas," *Bioelectromag.*, vol. 13, pp. 527–542, 1992.
[11] E. C. Jordan and K. G. Balmain, *Electromagnetic Waves and Radiating Systems*, 2nd ed. Englewood Cliffs, NJ: Prentice-Hall, 1968.
[12] C. A. Balanis, *Antenna Theory, Analysis and Design*, 2nd ed. New York: Wiley, 1997, pp. 416–422.
[13] *Handbook of Mathematical Functions*, M. Abramowitz and I. A. Segun, Eds., Dover, New York, 1968.

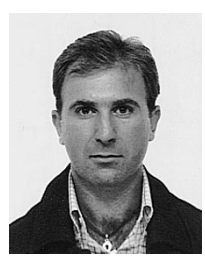

Antonio Faraone (M'97) was born in Rome, Italy, in April 1966. He received the laurea degree in electronics engineering (*magna cum laude*) in 1992 and the Ph.D. degree in applied electromagnetics in 1997, both from the University of Rome "La Sapienza," Rome.

Since 1997, he has been with Motorola Labs, Fort Lauderdale, FL, where he has been involved in theoretical and experimental research in antennas and RF dosimetry. His research interests include EMC and microwave integrated circuit full-wave modeling. He holds three patents and one is pending. He has authored or coauthored several scientific publications.

Dr. Faraone received the IEEE "Giorgio Barzilai" Prize for his laurea dissertation. He is a member of the International Union of Radio Science (URSI) and serves as a reviewer of several scientific journals.

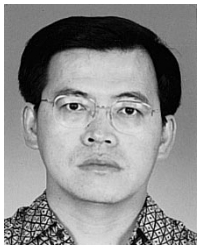

Roger Yew-Siow Tay (S'82–M'86) was born in Johor Baru, Malaysia, in 1958. He received the B.S. and M.S. degrees in electrical engineering from the University of Massachusetts, Lowell, in 1983 and 1985, respectively, and the Ph.D. degree from the Swiss Federal Institute of Technology (ETH), Zurich, Switzerland, in 1997.

In 1987, he joined the Research and Development Department, Motorola Electronics Pte. Ltd. (MEPL), Singapore. In 1990, he transferred to the Florida Electromagnetics Laboratory, Motorola, Inc., Fort Lauderdale, FL. In 1993, he was invited as an Academic Guest at ETH for eight months. He stayed with the Motorola Corporate Electromagnetics Laboratory as a Principal Staff Engineer until May 1998. He is currently a Senior Principal Staff Engineer in the Singapore Design Center of MEPL. He holds six patents and two are pending. He has contributed papers to several journals and conferences.

Dr. Tay is a member of the IEEE Antennas and Propagation and Electromagnetics Compatibility Societies. He is listed in *Marquis's Who's Who in Science and Engineering* and *Marquis's Who's Who in the World*. He was elected as a Science Advisory Board Associate at Motorola, Inc.

Ken H. Joyner was born in Melbourne, Australia, in 1949 and received the Ph.D. degree from La Trobe University, Melbourne, in 1975 for studies into radio-wave propagation via the ionosphere.

He held several teaching and university lectureships in Australia and overseas and returned to Australia in 1981 to lead the radio frequency and microwave research group at the Australian Radiation Laboratories. In 1985, he was appointed as a Principal Scientist at the Telecom Research Laboratories (TRL) and in 1989 was appointed as Head of the Electromagnetic Compatibility Section at TRL. In January 1997, he transferred to Motorola as Director of EME Strategy and Regulatory Affairs for the Asia-Pacific Region. His main research interests include the health and interference effects of mobile communications devices, measurement techniques, and the development and application of standards for the generation and transmission of electromagnetic energy (EME).

Dr. Joyner is the Australian Chairman of Commission K (Bioeffects and Medical Applications of Electromagnetic Fields) of the International Union of Radio Science (URSI) and has worked on numerous committees of Standards Australia in the development of human exposure standards, measurement standards, and technical performance standards. He has been a Member of the Royal Australian Air Force Specialist Reserve since 1984 and advises on the possible hazards to personnel, fuels, and ordnance from the military applications of EME and holds the rank of Wing Commander.

Quirino Balzano (S'63–M'72–SM'83) was born in Rome, Italy, in December 1940. In 1965, he received the Doctorate in Engineering degree in electronics from the University of Rome, Rome, Italy.

During 1966, he was at FIAT, SpA, Turin, Italy. From 1967 to 1974, he was with the Missile Systems Division, Raytheon Corporation. He was involved in the research and development of planar and conformal phased arrays. Since 1974, he has been with Motorola, Inc., Plantation, FL, where he is the Corporate Vice President and Director of the Florida Research Laboratories. His main interest is in the biological effects of human exposure to RF electromagnetic energy. He has written more than 50 papers on RF dosimetry near electromagnetic sources and the biological effects of RF energy. He has 27 patents in antenna and IC technology and has authored or coauthored more than 100 publications.

Dr. Balzano was on the Board of Directors of the Bioelectromagnetics Society, a scientific society dedicated to the research of the biological effects of electromagnetic fields. He received the IEEE Vehicular Technology Society Paper Prize Award in 1978 and 1982 and a certificate of merit from the Radiological Society of North America in 1981 for the treatment of tumors with RF energy. He is currently serving as Vice Chair of the Commission A of the International Union of Radio Science (URSI).